# Impaired bone fracture healing in type 2 diabetes is caused by defective functions of skeletal progenitor cells

| | |
|---|---|
| Journal: | *Stem Cells* |
| Manuscript ID | SC-20-0348.R3 |
| Manuscript Type: | Original Research |
| Date Submitted by the Author: | n/a |
| Complete List of Authors: | FIGEAC, Florence; Odense University Hospital, Endocrinology, KMEB<br>Tencerova, Michaela; Odense University Hospital, Endocrinology, KMEB; Czech Academy of Sciences, Molecular Physiology of Bone, Institute of Physiology<br>Ali, Dalia; Odense University Hospital, Endocrinology, KMEB<br>Andersen, Thomas; Odense University Hospital, Department of Pathology; University of Southern Denmark, Clinical Research; University of Southern Denmark, Department of Molecular Medicine<br>Appadoo, Dan Rémi; Odense University Hospital, Endocrinology, KMEB<br>Kerckhofs, Greet; UCLouvain, Biomechanics lab, Institute of Mechanics, Materials, and Civil Engineering; UCLouvain, Institute for Experimental and Clinical Research; KU Leuven, Department of Material Science and Engineering<br>Ditzel, Nicholas; Odense University Hospital, Endocrinology, KMEB<br>Kowal, Justyna; Odense University Hospital, Endocrinology, KMEB<br>Rauch, Alexander; Odense University Hospital, Endocrinology, KMEB; Odense University Hospital, Steno Diabetes Center Odense<br>Kassem, Moustapha; Odense University Hospital, Department of Endocrinology and Metabolism; University of Copenhagen, Department of Cellular and Molecular Medicine, Danish Stem Cell Center (DanStem) |
| Keywords: | Diabetes, Bone, Aging, Animal Models, Bone marrow stromal cells (BMSCs) |
| Journal Section: | Regenerative Medicine |
| Cell Types: | Bone Marrow Stem Cells, Mesenchymal Stem Cells |
| Diseases/Processes/Areas: | Diabetes, Obesity |
| | |

# Impaired bone fracture healing in type 2 diabetes is caused by defective functions of skeletal progenitor cells

***Running title**: Defective BM-MSCs in diabetic fracture*

Florence Figeac[1], Michaela Tencerova[1,2], Dalia Ali[1], Thomas L. Andersen[3,4,5], Dan Rémi Christiansen Appadoo[1], Greet Kerckhofs[6,7,8], Nicholas Ditzel[1], Justyna M. Kowal[1], Alexander Rauch [1,9], Moustapha Kassem[1,10]

*[1] Department of Molecular Endocrinology, KMEB, University of Southern Denmark and Odense University Hospital, DK-5000 Odense C, Denmark*
*[2] Current affiliation: Molecular Physiology of Bone, Institute of Physiology, the Czech Academy of Sciences, Prague, Czech Republic*
*[3] Department of Pathology, Odense University Hospital, DK-5000 Odense C, Odense*
*[4] Clinical Cell Biology, Research Unit of Pathology, Department of Clinical Research, University of Southern Denmark, DK-5000 Odense C, Denmark*
*[5] Department of Molecular Medicine, University of Southern Denmark, DK-5000 Odense C, Denmark*
*[6] Biomechanics lab, Institute of Mechanics, Materials, and Civil Engineering, UCLouvain, Louvain-la-Neuve, Belgium*
*[7] Institute for Experimental and Clinical Research, UCLouvain, Woluwe, Belgium*
*[8] Department of Material Science and Engineering, KU Leuven, Leuven, Belgium*
*[9] Steno Diabetes Center Odense, Odense University Hospital, Odense, Denmark*
*[10] Department of Cellular and Molecular Medicine, Danish Stem Cell Center (DanStem), University of Copenhagen, Copenhagen, Denmark*



**Authors contributions:**
Florence Figeac: Conception and design, financial support, provision of study material, collection of data, data analysis and interpretation, manuscript writing and final approval of manuscript
Michaela Tencerova: provision of study material, collection of data, data analysis and interpretation
Dalia Ali: collection of data, data analysis and interpretation
Thomas L. Andersen: collection of data, data analysis and interpretation
Dan Rémi Christiansen Appadoo: provision of study material, collection of data
Greet Kerckhofs: collection of data and interpretation
Nicholas Ditzel: provision of study material
Justyna Magdalena Kowal: provision of study material
Alexander Rauch: collection of data, data analysis and interpretation
Moustapha Kassem: Conception and design, financial support, data interpretation, manuscript writing and final approval of manuscript
All authors contributed with critical input on the manuscript draft and read and approved the final version of the manuscript.

**Corresponding author information**: Florence Figeac, Department of Molecular Endocrinology, KMEB, University of Southern Denmark and Odense University Hospital, DK-5000 Odense C, Denmark; tel.n.: 65504084; ffigeac@health.sdu.dk

This work was supported by a grant from Odense University Hospital grant (FF, 64-A3094), and grants from the NovoNordisk foundations (NNF150C0016284, NNF 180C0034186). A.R. was supported by a Lundbeck Fellowship (R335-2019-2195).

**Keywords:** Type 2 Diabetes, Bone healing, Insulin-resistance, Insulinopenia, Senescence

## Abstract

The mechanisms of obesity and type 2 diabetes (T2D)-associated impaired fracture healing are poorly studied. In a murine model of T2D reflecting both hyperinsulinemia induced by high fat diet (HFD) and insulinopenia induced by treatment with streptozotocin (STZ), we examined bone healing in a tibia cortical bone defect. A delayed bone healing was observed during hyperinsulinemia as newly formed bone was reduced by – 28.4±7.7% and was associated with accumulation of marrow adipocytes at the defect site +124.06±38.71%, and increased density of SCA1+ (+74.99± 29.19%) but not Runx2$^{+}$osteoprogenitor cells. We also observed increased in reactive oxygen species production (+101.82± 33.05%), senescence gene signature (≈106.66± 34.03%) and LAMIN B1$^{-}$ senescent cell density (+225.18± 43.15%), suggesting accelerated senescence phenotype. During insulinopenia, a more pronounced delayed bone healing was observed with decreased newly formed bone to -34.9± 6.2% which was inversely correlated with glucose levels ($R^2$=0.48, p<0.004) and callus adipose tissue area ($R^2$=0.3711, p<0.01). Finally, to investigate the relevance to human physiology, we observed that sera from obese and T2D subjects had disease state-specific inhibitory effects on osteoblast related gene signatures in human bone marrow stromal cells which resulted in inhibition of osteoblast and enhanced adipocyte differentiation. Our data demonstrate that T2D exerts negative effects on bone healing through inhibition of osteoblast differentiation of skeletal stem cells and induction of accelerated bone senescence and that the hyperglycaemia per se and not just insulin levels is detrimental for bone healing.

**Significance Statement**

Obesity and sedentary lifestyle increase risk for developing Type 2 Diabetes Mellitus (T2D). Among obesity and T2D complications is impaired bone fracture healing. The mechanisms leading to such complications are poorly studied. We examined tibia mono-cortical healing in insulin-resistance-obesity and T2D insulinopenic stages. We identified the contribution of the inhibition of a proper osteoblastic differentiation of the skeletal stem cells as well as the induction of a bone senescence environment to the impaired bone healing. The study also revealed that the hyperglycaemia per se and not just insulin levels is detrimental for bone healing.

## Introduction

Delayed union or non-union fracture healing are observed in 5 to 10% of all fractures and result in persistent pain, long-term disability and a need for second surgery, with high personal and socio-economic cost [1]. Obesity and type 2 diabetes (T2D) are important factors predisposing to this complication [2-4]. In addition, obesity and T2D are associated with increased bone fragility and fracture risk [5-8]. Also, the severity of skeletal fragility is positively correlated with poor glycemic control [9] and the presence of diabetic complications including microvascular disease [10-14].

The cellular and molecular mechanisms underlying defective bone healing in obesity and T2D, are poorly understood. Some studies have demonstrated the presence of a defective bone formation by osteoblastic cells in obese mice [15] and impaired angiogenesis as observed in osteoblast-specific VEGF$\alpha$-deficient mice [15-18]. In addition, it is not clear whether hyperglycemia or defective insulin signaling are the underlying mechanisms. Most studies have employed either genetic models e.g. *db/db* mice that are defective in leptin receptor signaling or obese mice induced by high fat diet (HFD) [19,20] as models of hyperinsulinemia and insulin-resistance. However, T2D is a heterogeneous disease characterized by a hyperinsulinemic phase caused by insulin resistance and an insulinopenic phase caused by pancreatic beta-cell failure [21]. The relative contribution of hyperinsulinemia versus insulinopenia to defective bone fracture healing, is not known.

Bone regeneration during fracture healing is mediated by skeletal stem and progenitor cells (also known as marrow stromal cells) (MSC) originating from bone marrow [22,23] or periosteum [24,25] with capacity for differentiation into bone forming osteoblastic cells (OB). Bone marrow (BM)-MSC differentiation to OB cells, is impaired in several clinical conditions known to be associated with defective bone regeneration e.g. aging and osteoporosis [26]. We have also recently reported that in obese hyperinsulinemic mice and humans, impaired OB differentiation of BM-MSC and enhanced differentiation to adipocytes are observed [27,28].

In the current study, we examined dynamics of bone fracture healing of a tibial cortical defect in a murine model of T2D reflecting both hyperinsulinemia caused by insulin resistance induced by HFD and insulinopenia induced by low doses streptozotocin (STZ) [29]. The tibial cortical defect model recapitulates phases of healing of a stabilized bone fracture [30]. We also examined the underlying cellular and molecular changes in MSC and bone microenvironment. To test the relevance to human physiology, the impact of sera from lean, obese and T2D patients was evaluated on the differentiation potential of hBM-MSCs.



## Materials & Methods

### *Animals*

Eight weeks old C57BL/6J male mice (C57BL/6JBomTac) from Taconic were housed under standard conditions (21°C, 55% relative humidity) on a 12-h light, 12-h dark cycle. Ad libitum food (Altromin® or D12492, Research Diets Inc.) and water were provided. All experimental animal procedures were approved by the Danish animal inspectorate (Dyreforsøgstilsynet) (2017-15-0201-01210).

### *Experimental design*

Experimental design is illustrated in figure 1A and figure 5A. Nighty male mice C57BL/6J were used for our first type of set up and divided accordingly to the experimental groups: (normal diet group (ND) n=45 and high fat diet group (HFD) n=45). In the HFD group, hyperinsulinemia was induced by 60% HFD feeding (Research Diets Inc D12492, containing 35% fat, 26% protein, 26% carbohydrate, 8.8% sucrose) from 8 weeks of age. Forty-eight male mice C57BL76J were used for our second set up and divided into 3 experimental groups (ND, HFD and HFD-STZ with n=16 for each). Insulinopenia was induced by 5 consecutive daily injection of low doses of Streptozotocin (STZ) (40 mg/kg body weight) 3 weeks after the start of the 60% HFD feeding

[29,31] for the HFD-STZ group. STZ was extemporaneously dissolved in ice cold 0.1M citrate buffer, pH 4.5. Control group (ND) and HFD were injected with vehicle alone: 0.1M citrate buffer, pH4.5.

***Monocortical tibial defect (MCTD)***

Under general anesthesia of 100 mg/kg ketamine and 10 mg/kg xylazine (i.p. injection), a monocortical tibia defect in the right leg of the mice, was performed as previously described [30,32,33]. In brief, the lateral aspect of the right tibia was exposed and by using a dental drill, a monocortical osseous hole of 0.8 mm diameter was created on the anterior surface of the tibia crest. Saline solution was used to remove bone dust and fragments from the defect. The anterior tibial muscle was restored into its anatomical position and skin was sutured. After surgery, oral Temgesic analgesia was administered.

***Body composition***

Body weight, total body fat and lean mass percentage were evaluated using dual-energy X-ray absorptiometry (DEXA) by using a PIXImus2® (version 1.44; Lunar Cooperation). DEXA scans were acquired on sedated mice.

***Glucose tolerance test (GTT)***

GTT was performed after overnight-fast and the mice were injected with D-glucose 1 g/kg intraperitoneally (i.p.) and glucose levels were measured at different time points using a BREEZE® 2 meter (Bayer®).

***Insulin concentration***

Insulin concentration was evaluated by Insulin Elisa (Thermofisher) in fasting blood serum collected at the end of the experiments.

***µ-CT imaging and analysis***

Bone healing was evaluated by *in vivo* µCT-imaging (vivaCT40 SCANCO Medical, Switzerland) with a voxel size of 10.5 µm at day (D)7, D14, D21 [30,34]. The defect region was defined between the interrupted cortical bone ends and a total of 80 slides (0.8 mm in length) covering most of the drilled cortical hole, were used for 3D reconstruction and analysis.

For the assessment of the Bone Marrow Adipose Tissue (BMAT) in the tibiae, we used contrast-enhanced µ-CT (CE-CT). For this, tibiae were fixed in formalin during 24 hours, were transferred to phosphate buffered saline (PBS) and were thereafter transferred to a polyoxometalate (POM)-based contrast solution (35mg of Hafnium-Wells Dawson POM per 1 ml PBS) [35]. Prior to the POM-staining, the distal ends of the bones were removed to allow better diffusion of the contrast solution into the bone marrow compartment. Samples were incubated in the contrast solution, while shaking gently, for 48 hours prior to CE-CT imaging. We used a Phoenix NanoTom M (GE Measurement and Control solutions, Germany) at a voltage of 60 kV and a current of 140 µA, and a 0.2 mm aluminum filter was used. The exposure time was 500 ms, and 1200 images were acquired over 360° (frame averaging = 3; image skip = 1). We scanned at a 2 µm isotropic voxel size. The BMAT volume was assessed in the proximal metaphysis starting directly underneath growth plate and covering a height of 1.2mm distal to the growth plate using CTAn (Bruker MicroCT, Belgium), as previously described [35].

***Isolation and culture of mouse BM-MSCs***

Cells were isolated as previously reported [27]. Briefly front and hind limbs were collected after 12 weeks HFD or 6 weeks HFD ± STZ, crushed and digested with 5% collagenase (StemCell). BM-MSCs were obtained as negative fraction from positive selection CD45+, CD31+ and Ter119+. BM-MSCs were cultivated and expanded *in vitro* in regular cell culture medium (alpha-MEM with 20% FBS, 1% Penicillin-Streptomycin and additives (Glutamax, MEM and sodium pyruvate). At passage 3 cells were used for differentiation studies.

***Mouse BM-MSCs In vitro differentiation studies***

At confluence, cells were switched to adipocyte differentiation medium (DMEM, containing 10% FBS, 10% horse serum (GIBCO), 100 U/mL penicillin (GIBCO), 100 µg/mL streptomycin (GIBCO), 100 nM dexamethasone (Sigma-Aldrich), 0.25 mM 3-isobutyl-1-methyxanthine (IBMX), 1 µM BRL (Sigma-Aldrich), 3 µg/mL insulin (Sigma-Aldrich)) or osteoblast differentiation medium (alpha MEM medium (GIBCO) containing 10% FBS, 100 U/mL penicillin (GIBCO), 100 µg/mL streptomycin (GIBCO) supplemented with 10 mM B-glycerophosphate (Sigma-Aldrich), 10 nM dexamethasone (Sigma-Aldrich), 50 µg/mL Vitamin C (Sigma-Aldrich) and 50 µg/mL Vitamin D (Sigma-Aldrich)). The media were changed every other day for the time of the experiment.

***Primary human BM-MSC collection and hMSC-TERT***

Human primary bone marrow stromal stem cells (hBM-MSCs) were isolated from bone marrow collected from lower extremities during routine surgeries at Department of Orthopedics and Traumatology, Odense University Hospital. Additional blood samples were collected from bone marrow donors and critical clinical data were obtained from the patient journal provided by the Danish healthcare system. The basic clinical information of donors is available in the **Supplementary Table 1.** All subjects received oral and written information and signed a consent. The project was approved by Scientific Ethical Committee of region of Southern Denmark (project ID: S-20160084). The detailed method for isolation and characterization of hBM-MSCs are provided elsewhere [36]. Briefly, hBM-MSCs were isolated based on gradient centrifugation and plastic adherence method. The cells were cultured in standard culture conditions and investigated for their biological functions including in vitro proliferation capacity, CD marker expression and differentiation ability. Osteogenic differentiation was induced in either a hMSC-TERT cell line immortalized by ectopic expression of telomerase reverse transcriptase gene (hTERT) [37] or hBM-MSC from lean patients (n=4).

***Human BM-MSCs In vitro differentiation studies***

*Adipocyte differentiation*

Cells were plated at a density of 30000 cells/cm$^2$. Adipocytic induction media DMEM, containing either 10% FBS (Gibco), or 5% FBS plus 5% of pooled 2 patients sera age/sex matched lean, obese or T2D subjects, 100 U/ml penicillin (Gibco), 100 μg/ml streptomycin (Gibco), 100 nM dexamethasone (Sigma-Aldrich), 0.5 mM 3-isobutyl-1-methyxanthine (IBMX), 1μM BRL (Sigma-Aldrich), 2μg/ml Insulin (Sigma-Aldrich), was changed every other day for 10 days. Adipogenic potential was evaluated by Oil red O staining. In brief at day 10 cells were fixed and stained with Oil Red O (Sigma-Aldrich) to visualize the lipid content.

*Osteoblast differentiation*

The cells were plated at a density of 20000 cells/cm$^2$. Osteogenic induction media a-MEM medium (Gibco) containing either 10% FBS or 5% FBS plus 5% of pooled 2 patients sera age/sex matched lean, obese or T2D subjects, 100 U/ml penicillin (Gibco), 100 μg/ml streptomycin (Gibco), 10 mM B-glycerophosphate (Sigma-Aldrich), 10 nM dexamethasone (Sigma-Aldrich), 50 μg/ml Vitamin C (Sigma-Aldrich) and 10mM Vitamin D3 (Sigma-Aldrich) was changed every other day. Osteogenic potential was evaluated by ALP activity assay at day 7 and by RNA-seq at day 10 of cultivation.

***Cellular reactive oxygen Species (ROS) detection assay***

Intracellular ROS level was evaluated with 2,7-dichloro-dihydro-fluorescein diacetate (DCFDA) (Abcam). The cells were seeded at 2.5x10$^4$ cells/well. After 24 hours, culture media was replaced with DMEM complete media without phenol red supplemented with tert-butyl hydrogen peroxide (TBHP) at 100μM for 2 hours. Media with TBHP was removed and cells were loaded with DCFDA 25μM and incubated for 45 minutes at 37°C. DCFDA was removed and experimental conditions (media with or without TBHP) were added again to the cells. Then, the fluorescent intensity was measured at Excitation 485 nm and Emission 535 nm kinetically using microplate reader every 1 minute for 30 minutes.

***RNA extraction and real time qRT-PCR***

DNase I treated RNA was reverse transcribed using a High Capacity cDNA Reverse Transcription Kit (Applied Biosystems). Quantitative real-time PCR was performed with an Applied Biosystems 7500 Real-Time PCR System using Fast SYBR Green Master Mix (Applied Biosystems) with specific primers (**Supplementary Table 2**). 36B4 was used as housekeeping genes for normalization of gene expression.

***Analyses of gene expression by RNA-seq***

Primary human BM-MSCs were exposed for 10 days to osteogenic induction media containing 5% FBS plus 5% of serum that was pooled from 2 lean, obese or T2D subjects, who are age and sex matched. RNA was extracted in TRIzol (Thermo Fisher) and RNA-seq was performed according to manufacturer's instructions (TruSeq 2, Illumina) using 1 µg RNA for preparation of cDNA libraries. Sequencing reads were mapped to the human genome (GRCh38) using STAR [38] and tag counts were summarized at the gene level using HOMER [39]. Differentially expressed genes between the three conditions were determined by DESeq2 [40] using a threshold of an adjusted p-value (FDR) below 0.01. Gene ontology analysis was performed using goseq [41] and pathway enrichment analysis was done using a hypergeometric test with gene sets from the SPEED2 pathway [42]. Overlap of gene set were determined using a jaccard index.

***Histology and histomorphometry***

Formalin fixed samples were decalcified in EDTA and embedded in paraffin. Longitudinal sections (4µm) including the defect region (identified by interrupted cortical bone ends) were cut, serially divided and stained for H&E, modified Masson´s Trichrome, and immunostaining (see below). Four sections per defect region were used to estimate the bone area and adipocyte area per tissue area. Sections were scanned with Hamamatzu scanner and analyzed using a point grid [38]. Within the region of interest (ROI) covering the defect region the number points upon bone, adipocytes and the remaining tissue area were counted, and used to calculate the percentage BV/TV and Ad.V/TV by dividing with the total number of points within the ROI.

***Immunohistochemistry***

Immunostainings were performed using a standard protocol. In brief, paraffin sections were deparaffinized, dehydrated and heat treated before incubated with primary antibody against Insulin (DAKO A0564), Sca1 (abcam ab51317) and Lamin B1 (abcam ab16048) followed by secondary detection (Anti-rabbit HQ: Ventana 760-4815), chromogen visualization (Anti-HQ HRP: Ventana 760-4820 and Purple-kit: Ventana 760-229) and counterstaining with hematoxylin. Based on the Insulin immunostaining, the β-cell area per tissue area in pancreas (4 sections from different depths) were estimated used Image J. Based on the SCA1 immunostaining the density of stem and osteoprogenitors cells per tissue area were counted and based on the Lamin B1 immunostaining the density of senescent Lamin B1 negative cells were counted [39]. A minimum of 2500 cells were evaluated for each condition per defect region.

***In situ hybridization***

In situ hybridization was performed on paraffin sections (3.5-mm thick) using an enhanced version of the RNAScope 2.5 high definition procedure (310035, ACD Bioscience, Newark, CA, US). Sections were deparaffinized, rehydrated and pretreated as previously [40], and hybridized overnight at 40C with 20-ZZ-pair probes (414021, ACD) targeting the mRNA of *Runx2* 3838-4821 (NM_001145920.2) and of Pdgfrα (Biotechne: RNAscope Probe, Mm-Pdgfra, ref 480661). A negative control only hybridized with probe diluent was included. Finally, the hybridized probe pairs were detected as previously described [40].

***Statistical analysis***

Data were analyzed with graph pad Prism 7 software (GraphPad). Results are expressed as mean ± (standard error of the mean (SEM) or standard deviation (SD) as appropriate. The difference between groups was examined using analysis of variance (ANOVA) followed by Sidak´s post hoc test and two-tailed unpaired Student´s t test.

# Results

### HFD-diet induces hyperinsulinemic T2D

Male mice fed ad libitum with either a high-fat diet (HFD) for 12 weeks exhibited increased body weight (28.85%±2.5), fat mass (154.7%±8.7) and decreased lean mass (26.9%±1.5) compared to those fed a normal diet (ND (**Figures 1A-D**). GTT showed impaired glucose tolerance in HFD mice compared to normal diet (ND) controls (**Figures 1E-F**). Also, measurement of insulin levels revealed a hyperinsulinemia in the HFD group (Figure 1G), which was consistent with the increased number of insulin-positive β -cell area (**Figures 1H-I**).

### Hyperinsulinemic T2D impairs bone fracture healing

To study the impact of hyperinsulinemic T2D on bone fracture healing, mice fed with HFD or ND were subjected to a tibial monocortical defect and rate of bone regeneration was determined by µCT scanning at day (D)-7, D14 and D21 (**Figure 1A**). A decrease in the newly formed bone was observed in the HFD group at D14 and maintained at D21 (**Figures 2A-B**). Similarly, histomorphometric analysis (**Figure 2C**), revealed decreased callus bone volume per tissue volume (BV/TV) in the HFD group (D7) (**Figure 2D**). Since HFD increases bone marrow adiposity (BMA) [27], we determined callus adipose volume per tissue volume (AdV/TV) area and observed a significant increase (D14) (**Figures 2C and 2E**). Also, callus AdV/TV was negatively correlated with callus BV/TV (**Figures 2F)**.

### HFD-induced T2D impairs osteoprogenitor cell differentiation

To determine the cellular mechanisms of impaired bone regeneration in hyperinsulinemic T2D mice, the density of SCA1+ stem and osteoprogenitor cells identified, and *Runx2+* osteoblastic cells, respectively, were determined at D7 during bone regeneration (**Figure 1A**), by immunochemistry staining and *in situ* hybridization (ISH). The density of $SCA1^{+}$ osteoprogenitors but not *Runx2+* osteoblastic cells was significantly increased in HFD group (**Figures 3A-C**). We also confirmed by flow cytometry that all isolated BM-MSCs from both groups expressed SCA1+ (**Figure 3D**) as previously reported [41], examined their differentiation

potential to osteoblastic and adipocytic cells and observed enhanced differentiation capacity to adipocytic but not to osteoblastic cells (**Figure 3E**).

**HFD-induced T2D leads to accelerated senescence of the bone marrow microenvironment**

Bone fracture induces oxidative stress [42] and patients with T2D are known to exhibit increased cellular oxidative stress due to accumulation of reactive oxygen species (ROS) [43].

Since increased oxidative stress leads to accelerated cellular senescence, we examined the presence of senescent cells *in vivo* at the callus area (**Figure 4A**) and we observed an increased density of LAMIN B1 negative ($LMNB1^-$) senescent cells in HFD group (**Figure 4B**). In addition, we examined the response of cultured BM-MSC to oxidative stress induced by $H_2O_2$ treatment and observed increased gene expression of senescence associated secretory phenotype (SASP) (**Figure 4C**) and cellular senescence gene markers: *p53*, *p16* and *p21* (**Figure 4D**), which were associated with increased ROS production (**Figure 4E**) in BM-MSC cells derived from HFD mice.

**STZ-treatment under HFD induces insulinopenic T2D**

Since insulin is known for its anabolic effects on bone [44,45], we tested whether the insulinopenic phase of T2D exerts differential effects on bone fracture healing. We employed a non-genetic mouse model of insulinopenic T2D. As shown in **Figure 5A**, mice were fed with ND or HFD for 1 month followed by daily injections for 5 days of low dose streptozotocin (STZ) or vehicle. Prior to STZ treatment, both groups fed HFD exhibited higher body weight compared to ND group. Following STZ injection, the HFD+STZ group lost weight compared to HFD group during 2 weeks follow up (**Figure 5B**). Also, animals in HFD+STZ group exhibited a pronounced impairment of glucose tolerance (**Figures 5C-D**) accompanied by a significant insulinopenia (Figure 5E) and β-cell mass reduction (**Figures 5F-G**) compared to the other groups.

**Insulinopenic T2D impairs bone fracture healing**

We observed the significantly decreased volume of newly formed bone in both HFD and HFD-STZ groups at D14 (**Figures 6A-B**) and this effect was more pronounced in the HFD-STZ group. The histomorphometric evaluation of the Adiposity volume per tissue volume (AdV/TV) in bone marrow of the proximal tibia revealed expansion in HFD group and to a lesser degree in HFD-STZ group where insulin levels were reduced (**Figures 6C-D**). Histomorphometric analysis also revealed decreased callus BV/TV in HFD and HFD-STZ groups (D7) (**Figures 6C and E**) and similar to µCT-scanning data, the decreased callus BV/TV was more pronounced in HFD-STZ group (**Figures 6C and 6E**). Callus AT area was increased to a similar extent in HFD and HFD-STZ groups (**Figures 6C and 6F**). Interestingly, AUC of GTT, reflecting the degree of hyperglycemia, was inversely correlated with the callus BV/TV (**Figure 6G**), and positively correlated with callus AdV/TV (**Figure 6H**). Also, callus AdV/TV area was negatively correlated callus BV/TV (**Figure 6I**).

**Osteoprogenitors and microenvironment in Insulinopenic T2D**

Since HFD is associated with enhanced bone marrow senescence (**Figure 4A**), we examined changes in density of senescent cells in HFD-STZ mice (**Figures 7A and C**). While hyperinsulinemia increased the density of senescent LMNB $B1^-$ cells in HFD group, the density of senescent cells was similar in HFD-STZ and control groups (**Figure 7C**) and the gene expression of *P16* in isolated BM-MSCs showed a statistically significant similar trend (**Figure 7D**). Finally, the density of SCA1+ cells was similar between HFD-STZ and control groups (**Figures 7B and E**) while the number of PDGFRα + cells tended to increase but there was no statistically significant difference between the groups (**Figures 7F-G**).

**Sera from diabetic patients with fractures impairs OB of human BM-MSC**

Our data suggest that T2D induces changes in the bone marrow microenvironment that lead to impaired bone regeneration through inhibition of BM-MSCs differentiation into OB cells. To corroborate these findings in humans, we used human sera as surrogate for the microenvironment to which BM-MSCs are exposed. We obtained sera from lean, obese patients and obese patients with T2D that were admitted to a local hospital

with bone fractures (for basic patient profile, see **Supplementary Table 1**) and tested their effects on osteoblast differentiation of a telomerized human BM-MSC cells line (hMSC-TERT) [37] and on adipocyte and osteoblast differentiation of primary human BM-MSC. As shown in **Figure 8A,** AD differentiation as evaluated by Oil red O staining was enhanced when the cells were treated with sera from obese and T2D patients whereas as shown in the **Figure 8B,** OB differentiation as evaluated by ALP activity, was inhibited. This inhibition was more pronounced in cells cultured in the presence of sera obtained from obese T2D patients. The observed reduced ALP activity effects were consistent in both hMSC-TERT and primary BM-MSC (**Figure 8B**). To identify mechanisms leading to the impaired osteogenic differentiation, we performed RNA-seq analysis on primary BM-MSCs undergoing osteoblast differentiation in presence of sera from either lean, obese or T2D subjects. PCA plot revealed a high similarity between replicates and separation of the three conditions (lean, obese, T2D) (**Supplementary Figure 1A**). Data analysis revealed differential expression of 791 genes across all conditions (**Figure 8C and Supplementary Figure 1C**). In general, we observed similar changes in gene expression comparing obese and T2D to lean (272 genes both up and 208 genes both down), but also identified genes with distinct expression patterns comparing T2D to obese (188 genes obese high and 123 genes T2D high). The latter two were mostly characterized by opposite expression patterns between obese and T2D versus lean (**Supplementary Figure 1B**). In line with the reduced differentiation capacity, gene ontology analysis revealed that genes being suppressed in BM-MSCs exposed to serum from obese and T2D subjects (both down) belong to bone pathway categories as extracellular matrix organization, skeletal system development, ossification, and osteoblast differentiation (**Figure 8D**). Interestingly, the differential gene expression in BM-MSCs incubated with serum from T2D compared to obese patients showed enrichment for osteoblast and collagen related terms while subjected to obese serum (obese high) and ion transport and lipid metabolism while subjected to T2D serum (T2D high). Further, bioinformatic analysis, reveal additional differences between gene expression pattern. We identified two sets of genes belonging to bone related GO terms: extracellular matrix organization, skeletal system development, ossification, and osteoblast differentiation. The first set of genes included genes with reduced expression in BM-MSCs with serum from

either obese or T2D patients (both down) e.g. *ATF4*, *CEBPA*, *IGF1*, *IGFBP5*, *SMAD3*, *SMAD6* and *SOX9* whereas the second set of genes were highly expressed in BM-MSCs with serum from obese patients (obese high) e.g. *IGF2*, *SFRP1*, *SPARC*, *TNFRSF11B*, *LRP1* as well as several genes coding for collagen proteins. Our data suggest additional impairment of ostogenic potential takes place during transition from obesity to T2D (**Supplementary Figure 2**). In order to test for the existance of differences in the activated pathways in BM-MSCs exposed to obese versus T2D patients serum, we observed that the two sets of genes respond to similar signalling pathways: TGFβ, Insulin, TNFα, and HIPPO. However, genes that exhibited decreased gene expression (both down), were more likely to be regulated by JAK-STAT, VEGF, MAPK and IL1 signaling compared to those with high expression levels in BM-MSCs treated with serum from obese subjects (obese high). The latter group of genes were more sensitive to Insulin and Hippo signaling. Thus, these gene groups have distinct preferences for the combinatorial activity of signaling pathways (**Figure 8F and Supplementary Figure 1D)**. Furthermore, pathway enrichment using SPEED2 database revealed that genes activated by key signals of osteoblast differentiation and bone formation including TGFβ, Insulin/MAPK+Pi3K, JAK-STAT, TNFα and HIPPO signaling, were downregulated in BM-MSCs cultured with serum from obese and T2D subjects (**Figure 8E**). On the other hand, genes with increased expression levels were p53 responsive genes which are associated with the senescent microenvironment corroborating our *in vivo* murine findings (**Figure 7**). Taken together these analyses demonstrate that the combinatorial action of signaling events elicited by the obese and type 2 diabetic microenvironment control distinct gene sets related to osteoblast differentiation, bone formation and collagen synthesis. The milder impairment observed under the obese condition may be mediated by a counterregulatory activity in bone-related pathways that is lost during transition to the diabetic state.

## Discussion

Increased bone fragility and fracture risk are complications of obesity and T2D that may be caused by the metabolic changes observed in the disease e.g. low grade inflammation, compromised vascularity, and generation of advanced glycation end products (AGEs), all known to exert negative effects on bone cells and bone remodeling [7,27,28,46]. In the present study, we report that bone regeneration during fracture healing, is impaired in both hyperinsulinemic and hypo-insulinemic T2D through two different mechanisms with negative effect on osteoblastic cells. In hyperinsulinemic T2D, we observed a hypermetabolic state, leading to an accelerated OB cellular senescence whereas severe hyperglycemia mediates the negative effects of hypo-insulinemic T2D on OBs.

T2D is a heterogenous disorder with patients presenting with insulin resistance and hyperinsulinemia or insulinopenia which is usually a sign of a longstanding disease [21]. However, most of the studies examining the biology of diabetic bone disease employ models with distinct genetic mutations, which does not reflect the pathophysiology of human T2D [20,47-49]. In the present study, we employed two mice models reflecting the heterogeneity of T2D phenotype: (i) HFD-induced obesity, insulin resistance and hyperinsulinemia, and (ii) HFD combined with STZ treatment that induced insulinopenia. The HFD-STZ model has previously been employed in studying the metabolic effects of antidiabetic and lipid lowering medications [31,50]. We extended these studies by examining the effects of T2D hyper-insulinemia and hypo-insulinemia on *in vivo* bone regeneration during healing of a monocortical tibial defect model that recapitulates phases of fracture healing of a stable fracture [30]. This model has the advantage of causing less stress to the animals and allows for a more precise quantification of the volume of newly formed bone using μCT imaging [30].

Hyperinsulinemic T2D in mice led to impaired fracture healing and this was associated with impaired differentiation of BM-MSCs to osteoblastic cells as evidenced by: (i) increased number of SCA1+ and PDGFRα stem cells while the number of committed osteoprogenitor Runx2+ cells did not change suggesting an osteoblast differentiation block, and (ii) enhanced BM-MSCs differentiation into adipocytes but not to

osteoblasts and this was associated with increased marrow adipose tissue formation *in vivo*. Our study corroborates previous studies that showed significant regulatory effects of T2D on skeletal stem cell functions. For example, Tevlin et al., reported that under high fat diet, there was a reduction in the number of MSC present in the callus following femoral fracture [20] while Hamann et al. [51] reported increased SCA1+ stem cell number in Zucker diabetic fatty rats (ZDF) following femoral fracture. Abundant literature reports interest into SCA1 as markers to identify progenitor cells [20,41,51]. Even though SCA1 is not the most specific marker for skeletal stem cells we show that it is widely expressed in the BM-MSCs that we isolate as it has been previously reported by our group [41].

We have previously reported that HFD induced hyperinsulinemia leads to a hypermetabolic state within the bone marrow leading to accelerated senescence of the bone microenvironment, enhanced adipocyte differentiation and increased bone marrow adiposity (BMA)[27,28]. The relationship between insulin resistance, hyperinsulinemia and accelerated senescence is under investigation but may be caused by induction of low grade inflammation and enhanced pro-inflammatory cytokine production [28,52,53]. In the current study, we corroborated these findings and demonstrated the contribution of accelerated cellular senescence in the bone micro-environment to impaired fracture healing and this mechanism may be responsible for the negative effects of obesity and hyperinsulinemia on the skeleton [28,54]. In addition to the accelerated senescence of the skeleton reported here, accelerated senescence has been observed in multiple tissues e.g. cardiovascular, kidney and brain in obese and T2D patients [55,56].

Increased BMA has been reported in several mice models of T2D and obesity : e.g. *ob/ob, db/db* and TALLYHO/JngJ mice [35,57-59] as well as in some human studies involving T2D patients [60,61]. Our study extends these findings, and it demonstrates increased adiposity at the site of fracture callus and corroborates the observed increase in callus adiposity after a femoral fracture reported by Brown et al in a study employing an obese, insulin resistant HFD mouse model [15]. The increased callus adiposity suggests a shift in MSC

differentiation allocation to adipocytes and not osteoblasts, as reported in the current study and in a previous study [27].

Insulinopenic T2D is usually observed in patients with long-lasting T2D and these patients usually exhibit multiple late diabetes complications [21]. In our study, the impaired bone regeneration during fracture healing was more pronounced in the insulinopenic mice. Insulin exerts anabolic effects on bone and insulin signaling in the bone microenvironment is maintained in obese mice and humans [27,28]. Insulin exerts its effects via interaction with cognate receptor on osteoblastic cells [62,63] and is important for fracture healing [64]. In our model, insulinopenia was associated with a more pronounced hyperglycemia that was positively correlated with impaired bone formation suggesting a causal effect. The direct effects of hyperglycemia [65-67] as well as its indirect effects through the formation of glycation end-products (AGEs) [68,69] are known to inhibit bone formation and osteoblast differentiation. Interestingly in the insulinopenic mice, the loss of peripheral adipose tissue was only accompanied by a minor decrease in BMA and no change in callus adiposity, suggesting that other factors, apart from insulin, are important for the maintenance of BMA. Our group has identified a number of secreted factors that are produced within the bone marrow micro-environment and play a role in lineage allocation of MSC into osteoblasts versus adipocytes [70-73]. These local factors may be important in the context of fracture healing and regulation of the local recruitment of osteoblastic cells during bone regeneration [70,71].

The role of changes in tissue microenvironmental composition in mediating impaired tissue homeostasis during aging and in a variety of diseases is increasingly recognized. Parabiosis experiments demonstrated that changes in composition of serum circulating factors led to defective tissue regeneration during aging of e.g. the heart, brain, muscle as well as bone [74-76]. We observed negative effects of sera obtained from obese and obese T2D patients with bone fractures, on osteoblast differentiation and enhancement of AD differentiation in hBM-MSCs supporting the hypothesis that factors present in BM microenvironment may affect the hBM-MSCs lineage allocation and differentiation choice contributing to

impaired bone formation. Similar to our finding, Deng et al [77] reported that diabetic serum with different levels of hyperglycemia inhibited osteoblastic differentiation of MSCs. Moreover RNA-seq performed on primary BM-MSCs undergoing osteoblastic differentiation in presence of the obese or T2D sera revealed 791 genes differentially expressed across all conditions. While the majority of genes exhibited similar pattern of response, we also observed distinct differences in gene expression patterns when comparing obese and T2D. GO enrichment analysis demonstrated downregulation of genes belonging to bone pathway categories as extracellular matrix organization, skeletal system development, ossification, and osteoblast differentiation, in both conditions. However, the differentially expressed set of genes enriched for osteoblast and collagen related terms were high under obese condition (obese high) and ion transport and lipid metabolism were high in T2D condition (T2D high). We have previously reported that obesity is associated with a hypermetabolic state with enhanced differentiation of BM-MSCs [28] which may explain the enhanced gene expression observed under the influence of obese sera.

Furthermore, pathway enrichment using SPEED2 database revealed downregulation of genes activated by several key pathways known for their essential role in osteoblast differentiation and bone formation including TGFβ [78,79], Insulin/MAPK+Pi3K [80,81], JAK-STAT [82], HIPPO [83] and upregulation for p53 responsive genes which are associated with cellular senescence [84]. Thus, RNA-seq data provide additional molecular explanation for the impairment of osteoblastic functions under obesity and T2D conditions.

Our study provides a working hypothesis for a personalized approach to improve fracture healing in patients with T2D based on their clinical phenotype. In obese hyperinsulinemia patients, enhanced insulin sensitivity and decreased insulin levels using metformin or insulin-sensitizers PPARγ agonists are recommended while in normal weight insulinopenic patients improving glycemic control through treatment with insulin should be the main focus. The clinical relevance and validity of this hypothesis remain to be determined in clinical studies.

## Acknowledgments

The authors are grateful to Lone Christiansen and Tina Kamilla Nielsen for excellent technical assistance and Carla Geeroms for the help with the CE-CT imaging and image analysis. Research data are not shared. Sequencing was carried out at the Villum Center for Bioanalytical Sciences, Functional Genomics & Metabolism Research Unit, University of Southern Denmark. We thank Tenna P. Mortensen and Ronni Nielsen for sequencing assistance.

## Disclosure of Potential Conflicts of Interest

The authors declare that there is no conflict of interest.

## Data Availability Statement

RNA sequencing and processed data have been deposited in the Gene Expression Omnibus (GEO) database, accession code will be provided upon review. Primary BM-MSCs were obtained from the orthopedic department during standard operation procedures with signed informed consent of the patients. The study was performed according to the Declaration of Helsinki, approved by the Scientific-Ethics committee at Odense University Hospital (S-20160084).

**Bibliography**


1 Holmes D. Closing the gap. Nature 2017;550(7677):S194-S195.

2 Hernandez RK, Do TP, Critchlow CW et al. Patient-related risk factors for fracture-healing complications in the United Kingdom General Practice Research Database. Acta Orthop 2012;83(6):653-660.

3 Neglia C, Argentiero A, Chitano G et al. Diabetes and Obesity as Independent Risk Factors for Osteoporosis: Updated Results from the ROIS/EMEROS Registry in a Population of Five Thousand Post-Menopausal Women Living in a Region Characterized by Heavy Environmental Pressure. Int J Environ Res Public Health 2016;13(11).

4 Zura R, Mehta S, Della Rocca GJ et al. Biological Risk Factors for Nonunion of Bone Fracture. JBJS Rev 2016;4(1).

5 Vestergaard P, Rejnmark L, Mosekilde L. Diabetes and its complications and their relationship with risk of fractures in type 1 and 2 diabetes. Calcif Tissue Int 2009;84(1):45-55.

6 Doucette CR, Horowitz MC, Berry R et al. A High Fat Diet Increases Bone Marrow Adipose Tissue (MAT) But Does Not Alter Trabecular or Cortical Bone Mass in C57BL/6J Mice. J Cell Physiol 2015;230(9):2032-2037.

7 Marin C, Luyten FP, Van der Schueren B et al. The Impact of Type 2 Diabetes on Bone Fracture Healing. Front Endocrinol (Lausanne) 2018;9:6.

8 Scheller EL, Khoury B, Moller KL et al. Changes in Skeletal Integrity and Marrow Adiposity during High-Fat Diet and after Weight Loss. Front Endocrinol (Lausanne) 2016;7:102.

9 Shibuya N, Humphers JM, Fluhman BL et al. Factors associated with nonunion, delayed union, and malunion in foot and ankle surgery in diabetic patients. J Foot Ankle Surg 2013;52(2):207-211.

10 Shanbhogue VV, Hansen S, Frost M et al. Bone disease in diabetes: another manifestation of microvascular disease? Lancet Diabetes Endocrinol 2017;5(10):827-838.

11 Jack M, Wright D. Role of advanced glycation endproducts and glyoxalase I in diabetic peripheral sensory neuropathy. Transl Res 2012;159(5):355-365.

12 Payne JF, Ray R, Watson DG et al. Vitamin D insufficiency in diabetic retinopathy. Endocr Pract 2012;18(2):185-193.

13 Waltenberger J. Impaired collateral vessel development in diabetes: potential cellular mechanisms and therapeutic implications. Cardiovasc Res 2001;49(3):554-560.

14 Yan X, Sano M, Lu L et al. Plasma concentrations of osteopontin, but not thrombin-cleaved osteopontin, are associated with the presence and severity of nephropathy and coronary artery disease in patients with type 2 diabetes mellitus. Cardiovasc Diabetol 2010;9:70.

15 Brown ML, Yukata K, Farnsworth CW et al. Delayed fracture healing and increased callus adiposity in a C57BL/6J murine model of obesity-associated type 2 diabetes mellitus. PLoS One 2014;9(6):e99656.

16 Hu K, Olsen BR. Osteoblast-derived VEGF regulates osteoblast differentiation and bone formation during bone repair. J Clin Invest 2016;126(2):509-526.

17 Lu C, Miclau T, Hu D et al. Ischemia leads to delayed union during fracture healing: a mouse model. J Orthop Res 2007;25(1):51-61.

18 Stegen S, van Gastel N, Carmeliet G. Bringing new life to damaged bone: the importance of angiogenesis in bone repair and regeneration. Bone 2015;70:19-27.

19 Fajardo RJ, Karim L, Calley VI et al. A Review of Rodent Models of Type 2 Diabetic Skeletal Fragility [in English]. Journal of Bone and Mineral Research 2014;29(5):1025-1040.

20 Tevlin R, Seo EY, Marecic O et al. Pharmacological rescue of diabetic skeletal stem cell niches [in English]. Sci Transl Med 2017;9(372).

21 Stidsen JV, Henriksen JE, Olsen MH et al. Pathophysiology-based phenotyping in type 2 diabetes: A clinical classification tool [in English]. Diabetes-Metab Res 2018;34(5).
22 Rickard DJ, Kassem M, Hefferan TE et al. Isolation and characterization of osteoblast precursor cells from human bone marrow. J Bone Miner Res 1996;11(3):312-324.
23 Chan CK, Seo EY, Chen JY et al. Identification and specification of the mouse skeletal stem cell. Cell 2015;160(1-2):285-298.
24 Debnath S, Yallowitz AR, McCormick J et al. Discovery of a periosteal stem cell mediating intramembranous bone formation. Nature 2018;562(7725):133-139.
25 Duchamp de Lageneste O, Julien A, Abou-Khalil R et al. Periosteum contains skeletal stem cells with high bone regenerative potential controlled by Periostin. Nat Commun 2018;9(1):773.
26 Kassem M, Marie PJ. Senescence-associated intrinsic mechanisms of osteoblast dysfunctions. Aging Cell 2011;10(2):191-197.
27 Tencerova M, Figeac F, Ditzel N et al. High-Fat Diet-Induced Obesity Promotes Expansion of Bone Marrow Adipose Tissue and Impairs Skeletal Stem Cell Functions in Mice. J Bone Miner Res 2018;33(6):1154-1165.
28 Tencerova M, Frost M, Figeac F et al. Obesity-Associated Hypermetabolism and Accelerated Senescence of Bone Marrow Stromal Stem Cells Suggest a Potential Mechanism for Bone Fragility. Cell Rep 2019;27(7):2050-2062 e2056.
29 Nath S, Ghosh SK, Choudhury Y. A murine model of type 2 diabetes mellitus developed using a combination of high fat diet and multiple low doses of streptozotocin treatment mimics the metabolic characteristics of type 2 diabetes mellitus in humans. J Pharmacol Toxicol Methods 2017;84:20-30.
30 Kim JB, Leucht P, Lam K et al. Bone regeneration is regulated by wnt signaling. J Bone Miner Res 2007;22(12):1913-1923.
31 Arulmozhi DK, Kurian R, Bodhankar SL et al. Metabolic effects of various antidiabetic and hypolipidaemic agents on a high-fat diet and multiple low-dose streptozocin (MLDS) mouse model of diabetes. J Pharm Pharmacol 2008;60(9):1167-1173.
32 Minear S, Leucht P, Jiang J et al. Wnt proteins promote bone regeneration. Sci Transl Med 2010;2(29):29ra30.
33 Minear S, Leucht P, Miller S et al. rBMP represses Wnt signaling and influences skeletal progenitor cell fate specification during bone repair. J Bone Miner Res 2010;25(6):1196-1207.
34 Leucht P, Jiang J, Cheng D et al. Wnt3a reestablishes osteogenic capacity to bone grafts from aged animals. J Bone Joint Surg Am 2013;95(14):1278-1288.
35 Kerckhofs G, Stegen S, van Gastel N et al. Simultaneous three-dimensional visualization of mineralized and soft skeletal tissues by a novel microCT contrast agent with polyoxometalate structure. Biomaterials 2018;159:1-12.
36 Kowal JM, Schmal H, Halekoh U et al. Single-cell high-content imaging parameters predict functional phenotype of cultured human bone marrow stromal stem cells. Stem Cells Transl Med 2020;9(2):189-202.
37 Simonsen JL, Rosada C, Serakinci N et al. Telomerase expression extends the proliferative life-span and maintains the osteogenic potential of human bone marrow stromal cells. Nat Biotechnol 2002;20(6):592-596.
38 Andreasen CM, Delaisse JM, van der Eerden BC et al. Understanding Age-Induced Cortical Porosity in Women: The Accumulation and Coalescence of Eroded Cavities Upon Existing Intracortical Canals Is the Main Contributor. J Bone Miner Res 2018;33(4):606-620.
39 Baar MP, Brandt RMC, Putavet DA et al. Targeted Apoptosis of Senescent Cells Restores Tissue Homeostasis in Response to Chemotoxicity and Aging. Cell 2017;169(1):132-147 e116.
40 Lassen NE, Andersen TL, Ploen GG et al. Coupling of Bone Resorption and Formation in Real Time: New Knowledge Gained From Human Haversian BMUs. J Bone Miner Res 2017;32(7):1395-1405.

41 Abdallah BM, Al-Shammary A, Skagen P et al. CD34 defines an osteoprogenitor cell population in mouse bone marrow stromal cells. Stem Cell Res 2015;15(3):449-458.
42 Turgut A, Gokturk E, Kose N et al. Oxidant status increased during fracture healing in rats. Acta Orthop Scand 1999;70(5):487-490.
43 Hamada Y, Fujii H, Fukagawa M. Role of oxidative stress in diabetic bone disorder. Bone 2009;45 Suppl 1:S35-38.
44 Klein GL. Insulin and bone: Recent developments. World J Diabetes 2014;5(1):14-16.
45 Sibai T, Morgan EF, Einhorn TA. Anabolic agents and bone quality. Clin Orthop Relat Res 2011;469(8):2215-2224.
46 Napoli N, Chandran M, Pierroz DD et al. Mechanisms of diabetes mellitus-induced bone fragility. Nat Rev Endocrinol 2017;13(4):208-219.
47 Roszer T, Jozsa T, Kiss-Toth ED et al. Leptin receptor deficient diabetic (db/db) mice are compromised in postnatal bone regeneration. Cell Tissue Res 2014;356(1):195-206.
48 Wallner C, Abraham S, Wagner JM et al. Local Application of Isogenic Adipose-Derived Stem Cells Restores Bone Healing Capacity in a Type 2 Diabetes Model. Stem Cells Transl Med 2016;5(6):836-844.
49 Wallner C, Schira J, Wagner JM et al. Application of VEGFA and FGF-9 enhances angiogenesis, osteogenesis and bone remodeling in type 2 diabetic long bone regeneration. PLoS One 2015;10(3):e0118823.
50 Li YG, Ji DF, Zhong S et al. Hypoglycemic effect of deoxynojirimycin-polysaccharide on high fat diet and streptozotocin-induced diabetic mice via regulation of hepatic glucose metabolism. Chem Biol Interact 2015;225:70-79.
51 Hamann C, Goettsch C, Mettelsiefen J et al. Delayed bone regeneration and low bone mass in a rat model of insulin-resistant type 2 diabetes mellitus is due to impaired osteoblast function. Am J Physiol Endocrinol Metab 2011;301(6):E1220-1228.
52 Kharas MG, Okabe R, Ganis JJ et al. Constitutively active AKT depletes hematopoietic stem cells and induces leukemia in mice. Blood 2010;115(7):1406-1415.
53 Schmitt TL, Hotz-Wagenblatt A, Klein H et al. Interdependent regulation of insulin receptor kinase activity by ADP and hydrogen peroxide. J Biol Chem 2005;280(5):3795-3801.
54 Farr JN, Khosla S. Cellular senescence in bone. Bone 2019;121:121-133.
55 Barzilai N, Huffman DM, Muzumdar RH et al. The critical role of metabolic pathways in aging. Diabetes 2012;61(6):1315-1322.
56 Palmer AK, Tchkonia T, LeBrasseur NK et al. Cellular Senescence in Type 2 Diabetes: A Therapeutic Opportunity. Diabetes 2015;64(7):2289-2298.
57 Turner RT, Kalra SP, Wong CP et al. Peripheral leptin regulates bone formation. J Bone Miner Res 2013;28(1):22-34.
58 Lindenmaier LB, Philbrick KA, Branscum AJ et al. Hypothalamic Leptin Gene Therapy Reduces Bone Marrow Adiposity in ob/ob Mice Fed Regular and High-Fat Diets. Front Endocrinol (Lausanne) 2016;7:110.
59 Devlin MJ, Van Vliet M, Motyl K et al. Early-onset type 2 diabetes impairs skeletal acquisition in the male TALLYHO/JngJ mouse. Endocrinology 2014;155(10):3806-3816.
60 Sheu Y, Amati F, Schwartz AV et al. Vertebral bone marrow fat, bone mineral density and diabetes: The Osteoporotic Fractures in Men (MrOS) study. Bone 2017;97:299-305.
61 Zhu L, Xu Z, Li G et al. Marrow adiposity as an indicator for insulin resistance in postmenopausal women with newly diagnosed type 2 diabetes - an investigation by chemical shift-encoded water-fat MRI. Eur J Radiol 2019;113:158-164.
62 Thomas DM, Hards DK, Rogers SD et al. Insulin receptor expression in bone. J Bone Miner Res 1996;11(9):1312-1320.
63 Thrailkill KM, Lumpkin CK, Jr., Bunn RC et al. Is insulin an anabolic agent in bone? Dissecting the diabetic bone for clues. Am J Physiol Endocrinol Metab 2005;289(5):E735-745.

64 Gandhi A, Beam HA, O'Connor JP et al. The effects of local insulin delivery on diabetic fracture healing. Bone 2005;37(4):482-490.
65 Garcia-Hernandez A, Arzate H, Gil-Chavarria I et al. High glucose concentrations alter the biomineralization process in human osteoblastic cells. Bone 2012;50(1):276-288.
66 Jiao H, Xiao E, Graves DT. Diabetes and Its Effect on Bone and Fracture Healing. Curr Osteoporos Rep 2015;13(5):327-335.
67 Ogawa N, Yamaguchi T, Yano S et al. The combination of high glucose and advanced glycation end-products (AGEs) inhibits the mineralization of osteoblastic MC3T3-E1 cells through glucose-induced increase in the receptor for AGEs. Horm Metab Res 2007;39(12):871-875.
68 Alikhani M, Alikhani Z, Boyd C et al. Advanced glycation end products stimulate osteoblast apoptosis via the MAP kinase and cytosolic apoptotic pathways. Bone 2007;40(2):345-353.
69 Sanguineti R, Storace D, Monacelli F et al. Pentosidine effects on human osteoblasts in vitro. Ann N Y Acad Sci 2008;1126:166-172.
70 Abdallah BM, Figeac F, Larsen KH et al. CRMP4 Inhibits Bone Formation by Negatively Regulating BMP and RhoA Signaling. J Bone Miner Res 2017;32(5):913-926.
71 Figeac F, Andersen DC, Nipper Nielsen CA et al. Antibody-based inhibition of circulating DLK1 protects from estrogen deficiency-induced bone loss in mice. Bone 2018;110:312-320.
72 Jafari A, Qanie D, Andersen TL et al. Legumain Regulates Differentiation Fate of Human Bone Marrow Stromal Cells and Is Altered in Postmenopausal Osteoporosis. Stem Cell Reports 2017;8(2):373-386.
73 Kristensen LP, Chen L, Nielsen MO et al. Temporal profiling and pulsed SILAC labeling identify novel secreted proteins during ex vivo osteoblast differentiation of human stromal stem cells. Mol Cell Proteomics 2012;11(10):989-1007.
74 Baht GS, Silkstone D, Vi L et al. Exposure to a youthful circulaton rejuvenates bone repair through modulation of beta-catenin. Nat Commun 2015;6:7131.
75 Katsimpardi L, Litterman NK, Schein PA et al. Vascular and neurogenic rejuvenation of the aging mouse brain by young systemic factors. Science 2014;344(6184):630-634.
76 Rebo J, Mehdipour M, Gathwala R et al. A single heterochronic blood exchange reveals rapid inhibition of multiple tissues by old blood. Nat Commun 2016;7:13363.
77 Deng X, Xu M, Shen M et al. Effects of Type 2 Diabetic Serum on Proliferation and Osteogenic Differentiation of Mesenchymal Stem Cells. J Diabetes Res 2018;2018:5765478.
78 Derynck R, Akhurst RJ. Differentiation plasticity regulated by TGF-beta family proteins in development and disease. Nat Cell Biol 2007;9(9):1000-1004.
79 Wu M, Chen G, Li YP. TGF-beta and BMP signaling in osteoblast, skeletal development, and bone formation, homeostasis and disease. Bone Res 2016;4:16009.
80 Ferron M, Wei J, Yoshizawa T et al. Insulin signaling in osteoblasts integrates bone remodeling and energy metabolism. Cell 2010;142(2):296-308.
81 Pramojanee SN, Phimphilai M, Chattipakorn N et al. Possible roles of insulin signaling in osteoblasts. Endocr Res 2014;39(4):144-151.
82 Sanpaolo ER, Rotondo C, Cici D et al. JAK/STAT pathway and molecular mechanism in bone remodeling. Mol Biol Rep 2020;47(11):9087-9096.
83 Yang W, Han W, Qin A et al. The emerging role of Hippo signaling pathway in regulating osteoclast formation. J Cell Physiol 2018;233(6):4606-4617.
84 Liu H, Li B. p53 control of bone remodeling. J Cell Biochem 2010;111(3):529-534.

## Figure Legends:

**Figure 1: Mice on high fat diet (HFD): body composition and glucose metabolism.**

(**A**) Study design depicting male mice C57Bl/6 randomized to either ND (10% kcal from fat) or HFD (60% kcal from fat) for 12 weeks followed by monocortical tibia defect (MCTD) surgery and follow-up for 3 weeks. Bone fracture healing was quantitated by µCT-scanning and quantitative histology. (**B**) Body weight and composition as (**C**) fat and (**D**) lean mass percentage were evaluated after 12 weeks normal diet (ND) or high fat diet (HFD). (**E-F**) Glucose tolerance test (GTT) and area under the curve (AUC) calculated for each mouse. (**G**) Insulin concentration in serum. (**H**) Representative photomicrographs of islets from pancreas of ND and HFD animal stained by H&E (upper panel- scale bar: 100µm and Insulin staining of pancreas of ND and HFD mice. Scale bar: 2.5mm. (**I**) Quantified β-cell area expressed as percentage of tissue area. Data are presented as mean ± SEM (n=16) (**B to F**) and n=3 for (**G to I**). **p<0.01; ***p < 0.001 as compared to ND group.

**Figure 2: Bone fracture healing in hyperinsulinemic mice on high fat diet (HFD)**

(**A**) Representative 3D-reconstruction of mineralized bone formed in defect region (scale bar: 100µm). (**B**) Bone Volume per Total volume (defect volume) percentage (BV/TV) of mineralized bone in defect region as evaluated by µCT at day (D) D7, D14 and D21 respectively) (n=15, 10 then 5). (**C**) Photomicrographs illustrating fracture healing at D7 and D14 (modified Masson Trichrome stain), Scale bars: 250µm. (**D**) Callus BV/TV percentage at D7 and (**E**) Callus Adipose tissue volume per total (defect volume) (Ad.V/TV) percentage at D14 as evaluated in the callus area (n=6). (**F**) Correlation of Callus Ad.V/TV percentage and BV/TV percentage (D14). Data are presented as mean ± SEM. *p<0.05, **p < 0.01.

**Figure 3: Effects of HFD-induced obesity on bone marrow osteoprogenitors**

(**A**) Representative photomicrographs of *in Situ* Hybridization for *Runx2* and immunostaining for SCA1 of the callus area (D7) following tibial monocortical defect. Scale bars:100µm (*Runx2*), and SCA1, 100µm (upper panels) and 20µm (lower panels). (**B**) *Runx2* positive pixels density per marrow defect fraction in the defect area (Ar./T.Ar.) (n=5 per group). (**C**) Number of SCA1 positive cells per defect area (n=5 per group). (**D**) Representative expression of SCA1 marker in BM-MSCs from ND (grey line) and HFD (orange line) animals as compared to unstained cells (blue line) as evaluated by flow cytometry. (**E**) Osteoblast and adipocyte differentiation of cultured bone marrow osteoprogenitor cells evaluated by gene expression of osteoblasts: *Alkaline phosphatase* (*Alp*), *Runx2*, *Osteocalcin* (*Bglap), Osterix (Sp7)* and adipocytes*: peroxisome proliferator active receptor,* (*PPARg2)* and *Fsp27* presented as fold change (F.C) over undifferentiated cells (n=3 per group).Data are presented as mean ± SEM. *p<0.05.

**Figure 4: Bone marrow microenvironment and bone marrow osteoprogenitor cells isolated from mice on high fat diet (HFD) exhibited an accelerated senescence phenotype**

(**A**) Immunostaining for Lamin B1 (LMNB1) (a negative marker of cellular senescence), on tibial sections after bone fracture at day (D)7. Lack of staining (blue cells) is indicating senescent cells (black arrowhead). Scale bar: 250µm (two left panels) and 20µm (two right panels). (**B**) Quantification of the effect of the HFD on LMNB1 loss in the defect area (n=5 per group). Gene expression profile of (**C**) senescence-associated secretory phenotype (SASP) markers and (**D**) senescence in isolated BM-MSCs from ND and HFD mice and submitted to an oxidative stress (1h treatment with $H_2O_2$). (**E**) ROS production following 1h treatment with $H_2O_2$ (100 µM) in cultured BM-MSCs from ND and HFD mice. Data are presented as mean ± SEM (n= 4-5). *p<0.05, **p<0.01, ***p<0.001.

**Figure 5: Insulinopenic mice induced by high fat diet (HFD) and Streptozocin (STZ) treatment: body composition and metabolism.**
(**A**) Study design depicting male mice C57Bl/6 randomized to either ND (10% kcal from fat) or HFD (60% kcal from fat) for 3 weeks followed by treatment with either 5 daily injections of vehicle or STZ (40mg/kg) and then at week 14 monocortical tibia defect (MCTD) surgery and 2 weeks as follow up period. Bone fracture healing was examined by µCT-scanning and quantitative histology. (**B**) Body weight represented as percentage change from initial weight (Delta). (**C**) Glucose tolerance test (GTT) and (**D**) area under the curve (AUC) calculated for each mouse. (**E**) Insulin concentration in blood serum. (**F**) Representative photomicrographs of insulin staining of pancreas of ND, HFD and HFD-STZ mice. Scale bar: 500µm. (**G**) Quantified β-cell area expressed as percentage of total area. Data are presented as mean ± SEM (n=16 for **B-D**,n=3 for **E** and n=6 for **F-G**). *p<0.05; **p<0.01; ***p < 0.001 as compared to ND and #p<0.05, ##p<0.01 and ###p<0.001 as compared to HFD. HFD-STZ= high fat diet and Streptozocin.

**Figure 6: Bone fracture healing in hypo-insulinemic mice on high fat diet (HFD) and Streptozocin (STZ)**
(**A**) Representative 3D-reconstruction of mineralized bone formed in defect region (scale bar: 100µm). (**B**) Bone Volume per Total volume (defect volume) percentage (BV/TV) of mineralized bone in defect region as evaluated by µCT (n= 15 at day (D) 7 and n=10 at D14). **(C**) 3D-reconstruction of proximal tibia (trabecular elements and BMAT). Scale bar 250µm. Representative photomicrographs of proximal tibia (H&E stain, scale bars: 500µm) and fracture healing at D7 and D14 (Masson Trichrome stain, scale bars: 250µm). (**D**) Adipocytes volume per total volume (Ad.V/TV) percentage at D14 as evaluated at the proximal tibia area, (**E**) Callus bone percentage at D7, (**F**) Callus Adipose tissue volume per total (defect volume) (Ad.V/TV) percentage at D14 as evaluated in the callus area (n=5- 4 depths). (**G**) Correlation between glucose levels as estimated by area under the curve (AUC) of glucose tolerance test (GTT) and callus BV/TV percentage and (**H**) AUC and callus Ad.V/TV percentage then (**I**) Ad.V/TV percentage with callus BV/TV percentage as determined at D14. *p<0.05, **p<0.01, ***p<0.001 as compared with ND value and #p<0.05 as compared with HFD value.

**Figure 7: *In vivo* changes in osteoprogenitor cells in insulinopenic condition**
(**A**) Immunostaining for Lamin B1 (LMNB1) (a negative marker of cellular senescence) performed on tibial sections following bone fracture at day (D)7. Lack of staining is indicating senescent cells (black arrowhead). Scale bar: 250µm (left panels) and 20µm (right panels). (**B**) Representative photomicrographs of SCA1 immunostaining in the callus area (D7) following tibial monocortical defect. Scale bars: 250µm (left panels) and 25µm (right panels). (**C**) Quantification of the effect of the HFD versus HFD-STZ on LMNB1 negative cells in the defect area. (**D**) *P16* gene expression in isolated BM-MSCs from ND, HFD and HFD-STZ animals. (**E**) Number of SCA1 positive cells per defect area. Data are presented as mean ± SEM (n= 4-5). *p<0.05. (**F**) Representative photomicrographs of *in situ* hybridization for *Pdgfrα* in the defect area (D7) following tibial monocortical defect. Scale bar 250µm (left panels) and 50µm (right panels). (G) Number of *Pdgfrα* positive cells per defect area (n=5 per group). Data are presented as mean fold change (F.C.) over non-induced cells ± SEM (n=4). *p<0.05 and **p<0.01.

**Figure 8: Obese and diabetic sera affect osteoblastic differentiation of h-MSCs-TERT cell line and primary BM-MSCs**
(**A**) Adipocytic differentiation of human primary BM-MSCs treated with human sera obtained from lean, obese and T2D patients as observed by Oil Red O staining at day 10 and (**B**) Osteoblastic differentiation of human primary BM-MSCs and hMSC-TERT cell line treated with human sera obtained from lean, obese and type 2 diabetes (T2D) patients as determined by quantifying ALP activity at

day 7. (**C**) Scatter plot showing the log-2-fold changes in gene expression comparing BM-MSCs treated with serum from lean, obese and type 2 diabetes patients. Genes were selected based on differential expression (FDR < 0.01, DEseq2) between any condition. Number of genes are indicated, both up: white dots in upper right part, both down: white dots in lower left part, T2D high: red dots, Obese high: blue dots. (**D**) Heat map showing gene ontology enrichment for selected gene groups from the RNA-seq data. (**E**) Heat map showing pathway enrichment for selected gene groups from the RNA-seq data using SPEED2 database focusing on activated genes only. (**F**) Heat map showing the jaccard index for the overlap of genes that are activated by TGFβ from the selected gene groups from the RNA-seq data with other pathways from SPEED2 analysis. Data are presented as mean ± SEM (n=4). *p<0.05 and **p<0.01.

**Supplementary Figure 1: Obese and diabetic sera affect osteoblastic differentiation of primary BM-MSCs**

(**A**) PCA plot analysis showing the variance of the RNA-seq data from BM-MSCs treated with serum from lean, obese and type 2 diabetes patients. (**B**) Box plots quantifying the log-2-fold changes between all conditions for the 4 gene groups defined in Figure 8C. (**C**) Bar plot showing normalized gene expression levels (RPKM) for selected genes; *ITGA11* Integrin subunit alpha 11, *CXCL5* C-X-C motif chemokine ligand 5, *CD36* CD36 molecule, *COL15A1* Collagen type XV alpha 1 chain, *LEP* leptin, *ELN* elastin, and *IGF2* insulin-like growth factor 2. (**D**) Heat map showing the jaccard index for a one-by-one overlap of genes from both up (left), both down (middle left), T2D high (middle right) and Obese high (right) that are activated by pathways from SPEED2 analysis.

**Supplementary Figure 2: Bone related gene ontology categories**

Heatmap showing the log 2-fold changes of genes from bone related gene ontology categories and that are differentially expressed (FDR < 0.01, DEseq2) comparing any condition. Genes are ordered according to binary clustering of membership in gene ontology categories (only the categories both down and obese high are displayed).

**FIGURE 1**

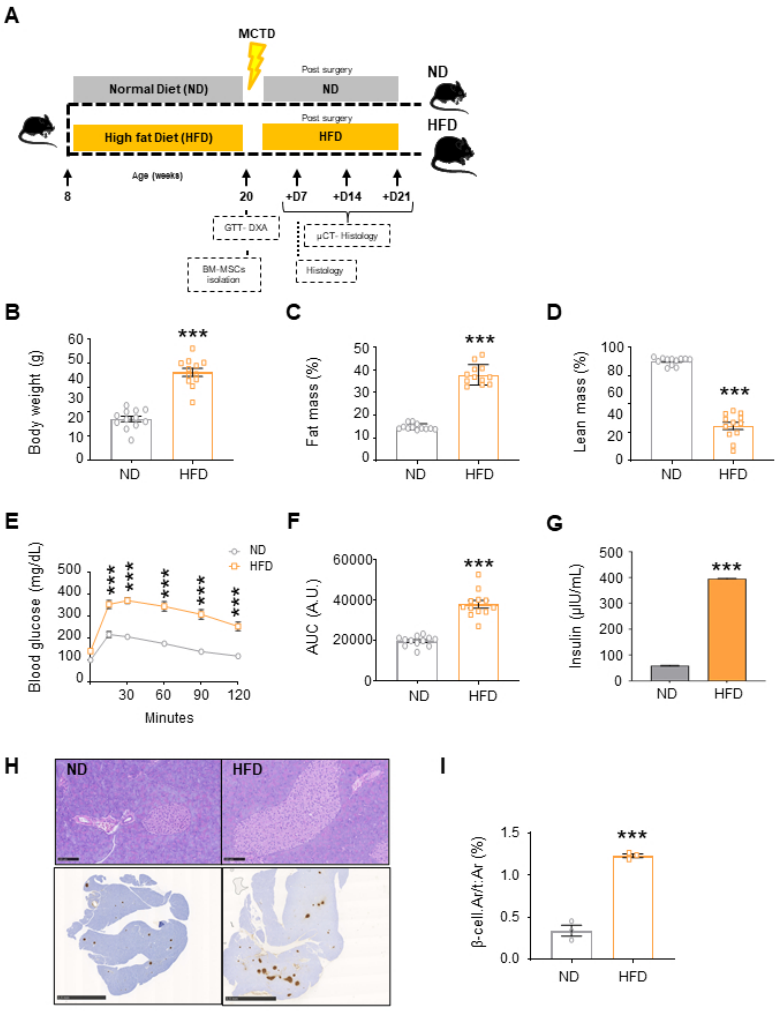


Figure 1: Mice on high fat diet (HFD): body composition and glucose metabolism.

190x275mm (96 x 96 DPI)

**FIGURE 2**

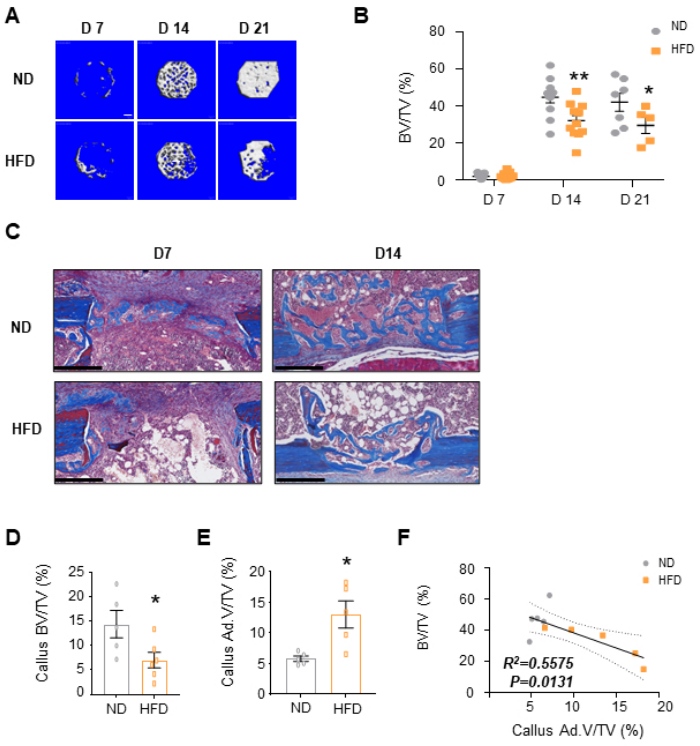


Figure 2: Bone fracture healing in hyperinsulinemic mice on high fat diet (HFD).

190x275mm (96 x 96 DPI)

**FIGURE 3**

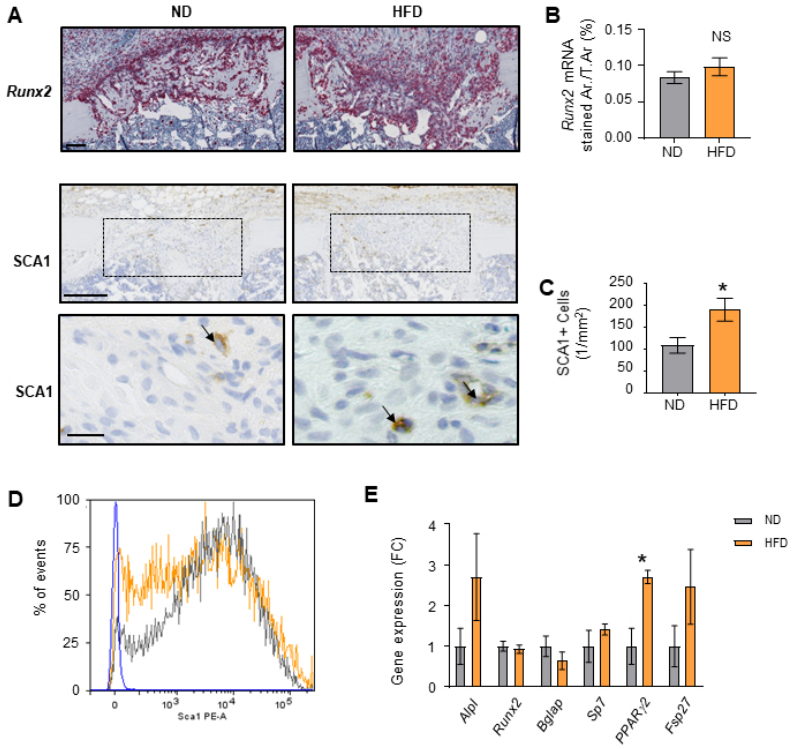


Figure 3: Effects of HFD-induced obesity on bone marrow osteoprogenitors.

190x275mm (96 x 96 DPI)

**FIGURE 4**

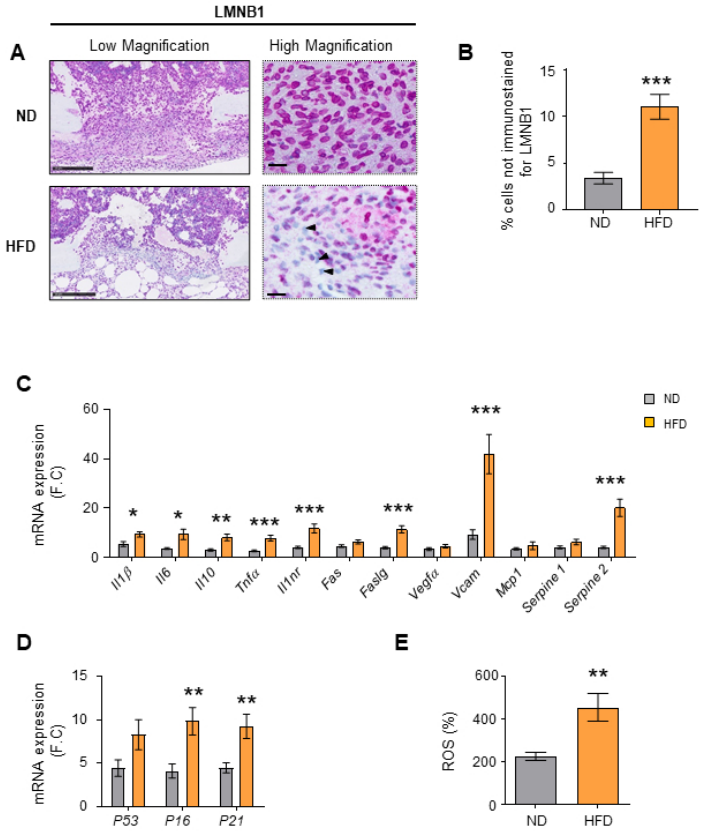


Figure 4: Bone marrow microenvironment and bone marrow osteoprogenitor cells isolated from mice on high fat diet (HFD) exhibited an accelerated senescence phenotype.

190x275mm (96 x 96 DPI)

**FIGURE 5**

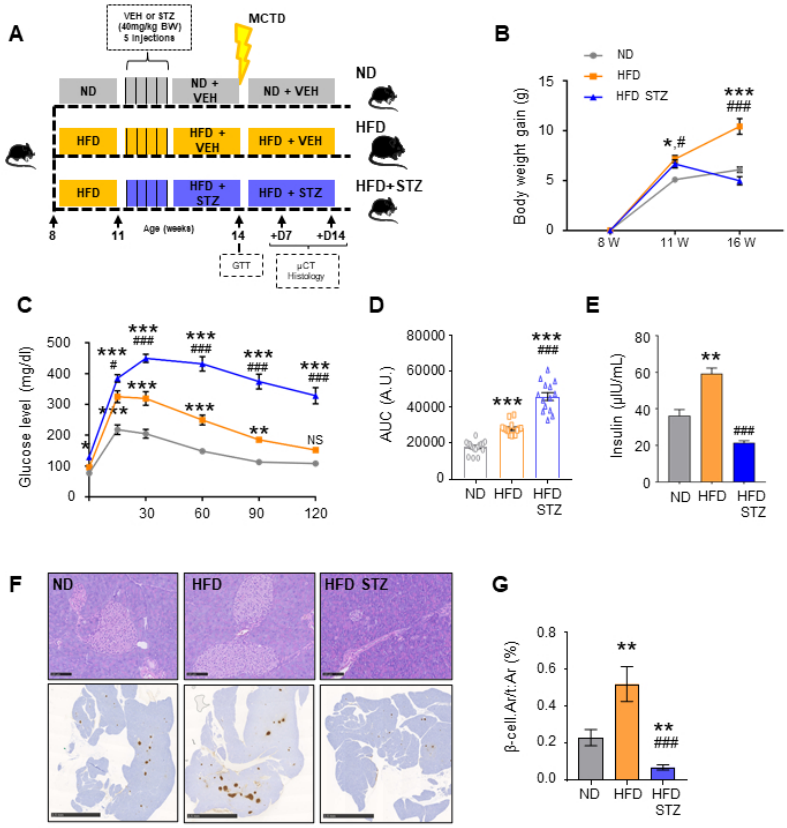


Figure 5: Insulinopenic mice induced by high fat diet (HFD) and Streptozocin (STZ) treatment: body composition and metabolism.

190x275mm (96 x 96 DPI)

**FIGURE 6**

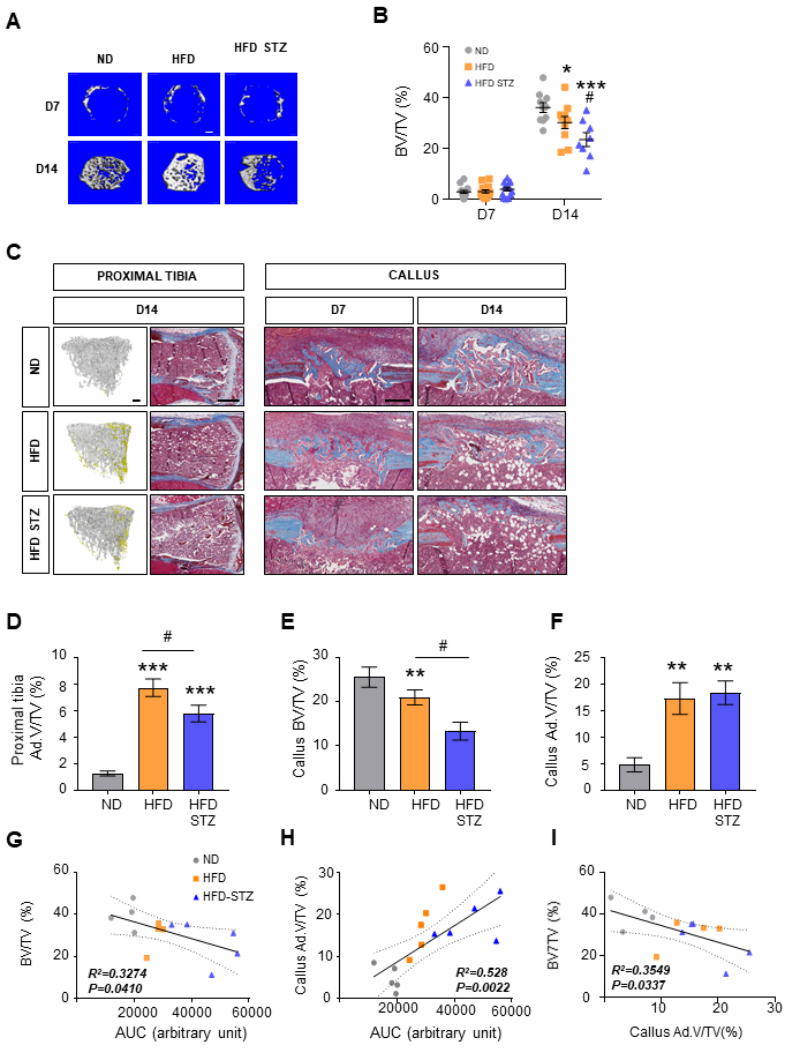


Figure 6: Bone fracture healing in hypo-insulinemic mice on high fat diet (HFD) and Streptozocin (STZ).

190x275mm (96 x 96 DPI)

**FIGURE 7**

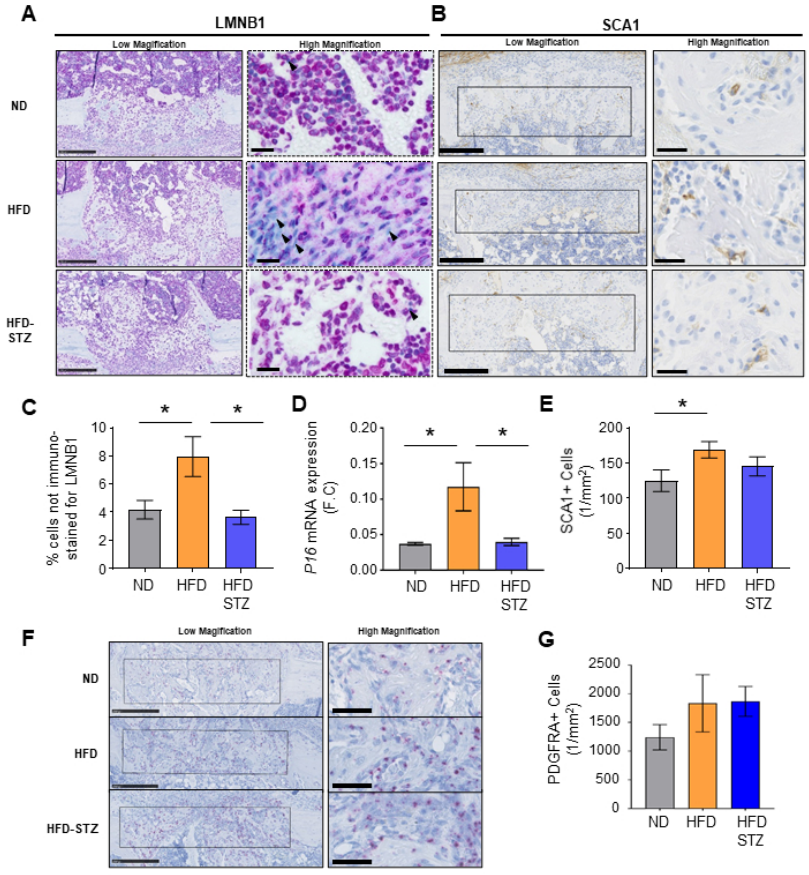


Figure 7: In vivo changes in osteoprogenitor cells in insulinopenic condition.

190x275mm (96 x 96 DPI)

**FIGURE 8**

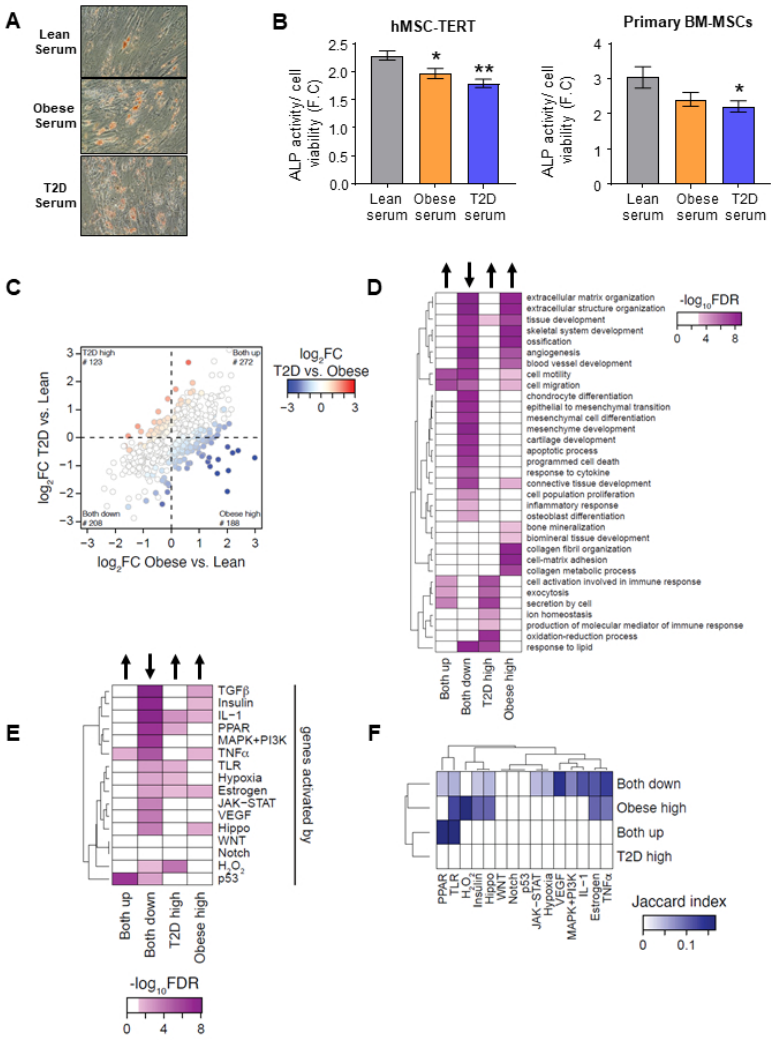


Figure 8: Obese and diabetic sera affect osteoblastic differentiation of h-MSCs-TERT cell line and primary BM-MSCs.

190x275mm (96 x 96 DPI)

**SUPPLEMENTARY FIGURE 1**

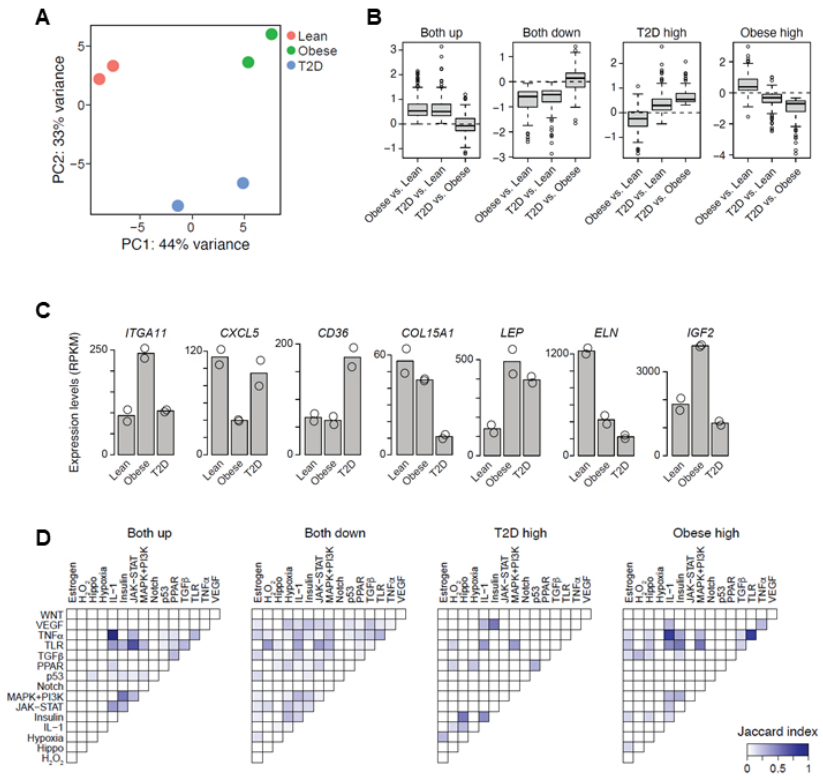


Supplementary Figure 1: Obese and diabetic sera affect osteoblastic differentiation of primary BM-MSCs
(A) PCA plot analysis showing the variance of the RNA-seq data from BM-MSCs treated with serum from lean, obese and type 2 diabetes patients. (B) Box plots quantifying the log-2-fold changes between all conditions for the 4 gene groups defined in Figure 8C.
(C) Bar plot showing normalized gene expression levels (RPKM) for selected genes; ITGA11 Integrin subunit alpha 11, CXCL5 C-X-C motif chemokine ligand 5, CD36 CD36 molecule, COL15A1 Collagen type XV alpha 1 chain, LEP leptin, ELN elastin, and IGF2 insulinlike growth factor 2. (D) Heat map showing the jaccard index for a one-by-one overlap of genes from both up (left), both down (middle left), T2D high (middle right) and Obese high (right) that are activated by pathways from SPEED2 analysis.

190x275mm (96 x 96 DPI)

## SUPPLEMENTARY FIGURE 2

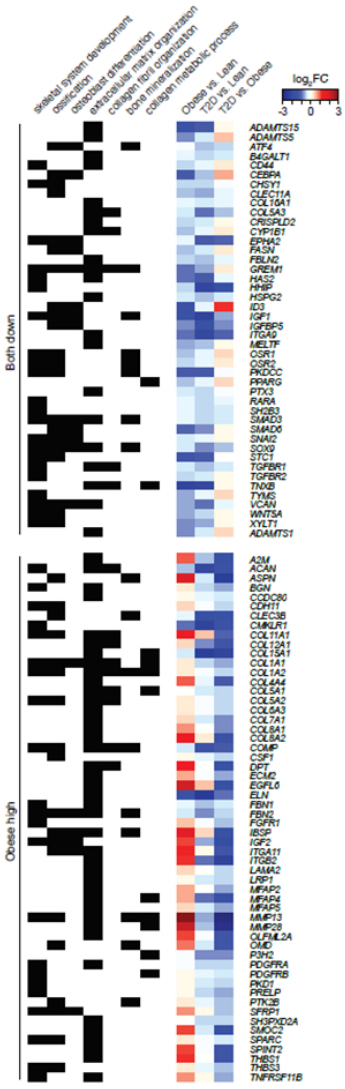


190x275mm (96 x 96 DPI)

**Supplementary Table 1**: Clinical characteristics of the BM-MSCs and sera donors

| | **Mean Age [range] (years)** | **Mean BMI [range] (kg/m²)** |
|---|---|---|
| **Cells´ donors** | 67.3 [44.0-80.0] | 22.20 [20.2-23.9] |
| **Lean serum´s donor** | 60.0 [55.0-69.0] | 22.5 [20.6-23.8] |
| **Obese serum´s donor** | 59.0 [58.0-60.0] | 33.2 [29.7-36.6] |
| **T2D serum´s donor** | 54.0 [42.0-66.0] | 32.4 [31.9-33.0] |

**Supplemental Table 2**. List of primer sequences used for qRT-PCR.

| Gene | Forward sequence | Reverse sequence |
|---|---|---|
| **Alpl** | GCCCTCTCCAAGACATATA | CCATGATCACGTCGATATCC |
| **Runx2** | AGCAACAGCAACAACAGCAG | GTAATCTGACTCTGTCCTTG |
| **Bglap** | CCTGAGTCTGACAAAGCCTTCA | GCCGGAGTCTGTTCACTACCTT |
| **Sp7** | AAGTTCACTTGCCTGCTCTGTT | TGCGCTGATGTTTGCTCAAG |
| **Pparγ2** | GGGTCAGCTCTTGTGAATGG | CTGATGCACTGCCTATGAGC |
| **Fsp27** | ATCAGAACAGCGCAAGAAGA | CAGCTTGTACAGGTCGAAGG |
| **P53** | TCTTATCCGGGTGGAAGGAAA | GGCGAAAAGTCTGCCTGTCTT |
| **p16** | GGGTTTTCTTGGTGAAGTTCG | TTGCCCATCATCATCACCT |
| **p21** | CCTGGTGATGTCCGACCTG | CCATGAGCGCATCGCAATC |
| **Il1β** | GCAACTGTTCCTGAACTCAACT | ATCTTTTGGGGTCCGTCAACT |
| **Il6** | GTTCTCTGGGAAATCGTGGA | TGTACTCCAGGTAGCTATGG |
| **Il10** | CTGGACAACATACTGCTAACCG | GGGCATCACTTCTACCAGGTAA |
| **Tnfα** | CCCTCACACTCAGATCATCTTCT | GCTACGACGTGGGCTACAG |
| **Il1rn** | GCTCATTGCTGGGTACTTACAA | CCAGACTTGGCACAAGACAGG |
| **Fas** | CTGCACCCTGACCCAGAATAC | ACAGCCAGGAGAATCGCAGTA |
| **Faslg** | CAGTCCACCCCCTGAAAAAAA | CCTTGAGTTGGACTTGCCTGTT |
| **Vegfα** | GTACCTCCACCATGCCAAGTG | TGGGACTTCTGCTCTCCTTCTG |
| **Vcam** | GGCTCCAGACATTTACCCAGTT | CATGAGCTGGTCACCCTTGAA |
| **Mcp1** | GCTGGAGAGCTACAAGAGGATCACC | TCCTTCTTGGGGTCAGCACAGAC |
| **Serpine 1** | GGACACCCTCAGCATGTTCA | CGGAGAGGTGCACATCTTTCT |
| **Serpine 2** | TTCCGCATACTGGAAACATCAG | GGATGCGTCCTCAATCTCATC |
| **36b4** | TCCAGGCTTTGGGCATCA | CTTTATCAGCTGCACATCACTCAGA |